

A Comparative Analysis of Image Descriptors for Histopathological Classification of Gastric Cancer

Marco Usai, Andrea Loddo, Alessandra Perniciano, Maurizio Atzori, Cecilia Di Ruberto

University of Cagliari, Cagliari, Italy

m.usai84@studenti.unica.it,

{andrea.loddo,alessandra.pernician,cecilia.dir,atzori}@unica.it

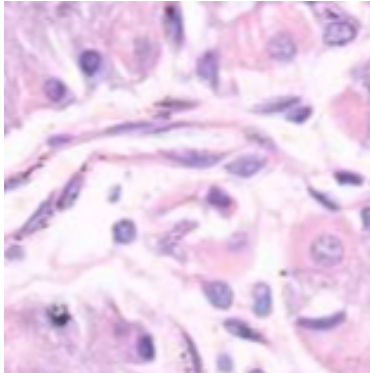
Abstract. Gastric cancer ranks as the fifth most common and fourth most lethal cancer globally, with a dismal 5-year survival rate of approximately 20%. Despite extensive research on its pathobiology, the prognostic predictability remains inadequate, compounded by pathologists' high workload and potential diagnostic errors. Thus, automated, accurate histopathological diagnosis tools are crucial. This study employs Machine Learning and Deep Learning techniques to classify histopathological images into healthy and cancerous categories. Using handcrafted and deep features with shallow learning classifiers on the GasHisSDB dataset, we offer a comparative analysis and insights into the most robust and high-performing combinations of features and classifiers for distinguishing between normal and abnormal histopathological images without fine-tuning strategies. With the RF classifier, our approach can reach F1 of 93.4%, demonstrating its validity.

Keywords: Gastric Cancer · Histopathological Images · Feature Extraction · Machine Learning · Convolutional Neural Networks

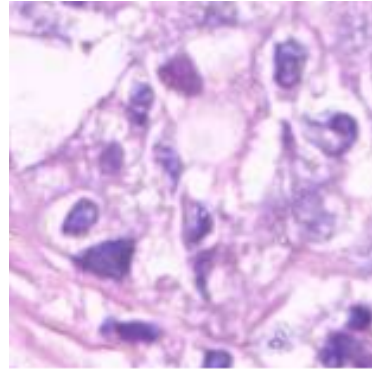
1 Introduction

Gastric cancer ranks as the fifth most common cancer worldwide and the fourth most lethal, with a global 5-year survival rate of approximately 20%. Despite extensive research into the disease's pathobiological parameters, predicting disease progression remains challenging, contributing to the low survival rate. Additionally, medical diagnostics' demanding and time-intensive nature can lead to critical details being overlooked during microscopic examinations, potentially resulting in incorrect diagnoses [8].

Developing computational tools capable of automatically and accurately performing histopathological diagnoses is crucial to mitigating the issues discussed. Recent advancements in computer technology, particularly in Machine Learning (ML) and Deep Learning (DL), have enabled significant progress in this area. This work explores classifying pathology images into two categories: healthy cells and tumor cells. The study employs various classifiers, extracts specific handcrafted (HC) features, and uses Convolutional Neural Network (CNN) architectures to extract deep features.



(a) Example of an image belonging to the normal class. It does not contain any cancerous regions.



(b) Example of an image belonging to the abnormal class, containing cancerous areas

Fig. 1: Sample images from the GasHisSDB dataset.

This study aims to evaluate the accuracy of shallow learning classifiers in classifying histopathological images using HC and deep features without employing specific fine-tuning strategies. Instead, it relies solely on deep features derived from pre-trained off-the-shelf CNNs.

This work’s key contributions include a comparative analysis of various HC and deep features with four ML classifiers and insights into the most robust and high-performing combinations of features and classifiers for distinguishing between normal and abnormal histopathological images.

2 Materials and Methods

2.1 Dataset

This work used the GasHisSDB dataset [7] as the benchmark. It is organized into three subfolders corresponding to different image sizes. This investigation focused on the 160×160 subfolder, comprising 33,284 tissue images belonging to the normal (20,160 images) and abnormal (13,124 images) classes. An image is categorized as normal if it lacks cancerous regions, indicating regular microscopic cell observations. Conversely, an image falls into the abnormal class if it contains more than 50% cancerous areas [9]. Figure 1 shows two image samples.

2.2 Image descriptors

HC features extracted from images encompass diverse descriptors aimed at deriving morphological, pixel-level, and textural information. As discussed by [16], these features are broadly classified into three categories: invariant moments, texture features, and color features. Below, we provide a concise overview of each category and the specific descriptors employed.

Invariant Moments - An image moment refers to a weighted average, denoted as the moment, of the pixel intensities within an image employed to extract specific properties. Moments find application in image analysis and pattern recognition to characterize segmented objects.

Chebyshev Moments (CH). These moments are a set of orthogonal moments [11] based on Chebyshev polynomials [4]. In this study, we employed first- and second-order moments, referred to as CH_1 and CH_2, respectively. Both were computed of order 5.

Second-order Legendre Moments (LM). These moments are derived from Legendre orthogonal polynomials [18, 17]. They capture and represent objects' shape and spatial characteristics within an image. In our analysis, we used Legendre moments of order 5.

Zernike Moments (ZM). First introduced by [13], Zernike moments are a set of orthogonal moments derived from Zernike polynomials. They are utilized to characterize the shape and structure of objects within an image. In this study, we applied Zernike moments of order 5 with a repetition of 5.

Texture features - They are particularly useful to emphasize fine textures.

Rotation-Invariant Haralick Features (HAR). Thirteen Haralick features [5] were extracted from the Gray Level Co-occurrence Matrix (GLCM) and subsequently converted into rotation-invariant features (refer to [15] for details). To ensure rotation invariance, four variations of the GLCM were computed, each with a distance parameter $d = 1$ and angular orientations $\theta = [0^\circ, 45^\circ, 90^\circ, 135^\circ]$.

Local Binary Pattern (LBP). LBP captures the texture and patterns present in an image, as outlined by [6]. In our study, we computed the histogram of the LBP, converting it to a rotation-invariant form [12], which was then extracted and utilized as the feature vector. The LBP map was generated within a neighborhood defined by a radius $r = 1$ and a number of neighbors $n = 8$.

Color features - They aim at extracting color intensity information from the images. In this study, these descriptors were calculated from images that underwent a conversion to grayscale, streamlining the process of analysis and computation.

Histogram Features. From the histogram that characterizes the overall color distribution within the image, we extracted seven statistical descriptors: mean, standard deviation, smoothness, skewness, kurtosis, uniformity, and entropy. These seven features are collectively referred to as *Hist*.

Autocorrelogram (AC). The AC integrates color information with the spatial correlation between colors [10]. Specifically, it records the probability of encountering two pixels of the same color at a distance d . In this study, we utilized four distinct distance values: $d = 1, 2, 3, 4$. The four resulting probability vectors are concatenated to form a comprehensive feature vector.

Haar Features (Haar). These features consist of adjacent rectangles with alternating positive and negative polarities, taking forms like edge features, line features, four-rectangle features, and center-surround features [19].

Deep features In the realm of ML learning, the combination of DL feature extraction and classification alongside shallow learning classifiers has proven to be a potent strategy for enhancing the predictive power of conventional DL models [2], also to overcome the obstacle of handling high-dimensional data.

In this context, CNNs have demonstrated their efficacy as feature extractors across various studies [1, 14]. CNNs excel at capturing comprehensive image features by passing input data through multiple convolutional filters, progressively reducing dimensionality across successive architectural layers. For our experiments, we opted for several pre-trained off-the-shelf architectures originating from the Imagenet1k dataset [3]. Detailed specifications regarding the selected layers for feature extraction, input dimensions, and the count of trainable parameters for each CNN model are outlined in Table 1.

Table 1: Employed CNN details including number of trainable parameters in millions, input shape, feature extraction layer, and related feature vector size.

Reference	Parameters (M)	Input shape	Feature layer	# Features
AlexNet	60	224×224	Pen. FC	4,096
DarkNet-19	20.8	224×224	Conv19	1,000
DarkNet-53	20.8	224×224	Conv53	1,000
DenseNet-201	25.6	224×224	Avg. Pool	1,920
EfficientNetB0	5.3	224×224	Avg. Pool	1,280
Inception-v3	21.8	299×299	Last FC	1,000
Inception-ResNet-v2	55	299×299	Avg. pool	1,536
ResNet-18	11.7	224×224	Pool5	512
ResNet-50	26	224×224	Avg. Pool	1,024
ResNet-101	44.6	224×224	Pool5	1,024
VGG19	144	224×224	Pen. FC	4,096
XceptionNet	22.9	299×299	Avg. Pool	2,048

2.3 Machine Learning Algorithms

This study’s HC and deep features serve as inputs for various ML classifiers. Let us provide a brief introduction to these classifiers.

Decision Tree (DT). A Decision Tree is a hierarchical data structure used for prediction. Each internal node represents a feature, with branches indicating possible feature values. The leaves denote different categories. The algorithm optimizes this structure by pruning nodes that contribute minimally to category separation, thus merging instances at higher levels. Classification is achieved by following the path from the root to a leaf node.

k-Nearest Neighbor (kNN). The kNN classifier categorizes observations by evaluating the classes of the k-training examples closest in distance to the observation in question. This method employs a local strategy to achieve classification by leveraging the proximity of neighboring instances. This work has set k equal to 3.

Support Vector Machine (SVM). SVM differentiates categories by mapping examples to distinct sides of a decision boundary. The one-vs-rest approach is used to handle multiclass problems, training individual classifiers to distin-

guish each class from all others. Here, a Gaussian radial basis function has been used as the kernel.

Random Forest (RF). This algorithm aggregates predictions from multiple decision trees, each built from random subsets of features and examples. By fostering diversity among the trees, this ensemble method enhances model robustness, improving resilience against data imbalance and mitigating overfitting. This work has set the number of DTs to 100.

2.4 Performance Evaluation Measures

To assess the performance of a binary classifier on a dataset, each instance is categorized as either negative or positive based on the classifier's predictions. The outcome of this classification, compared to the true target value, determines the contribution of each instance to the following measures:

- **True Negatives (TN):** instances from the negative class correctly predicted as negative.
- **False Positives (FP):** instances from the negative class incorrectly predicted as positive.
- **False Negatives (FN):** instances from the positive class incorrectly predicted as negative.
- **True Positives (TP):** instances from the positive class correctly predicted as positive.

Several performance measures have been used to evaluate classification performance. We now provide their definitions, tailored for binary classification tasks.

- **Accuracy (A):**

$$A = \frac{TP + TN}{TP + FN + FP + TN}$$

- **Precision (P):**

$$P = \frac{TP}{TP + FP}$$

- **Recall (R):**

$$R = \frac{TP}{TP + FN}$$

- **Specificity (S):**

$$S = \frac{TN}{TN + FP}$$

- **F1-score (F1):**

$$F1 = 2 \cdot \frac{P \cdot R}{P + R}$$

- **Matthew Correlation Coefficient (MCC):**

$$MCC = \frac{TP \cdot TN - FP \cdot FN}{\sqrt{(TP + FP)(TP + FN)(TN + FP)(TN + FN)}}$$

– **Balanced Accuracy (BACC):**

$$BACC = \frac{R + S}{2}$$

3 Experimental Results

In this section, we present the experimental results. The configuration of the experimental setup is detailed in Section 3.1. The outcomes obtained with the HC and deep features are discussed in Section 3.2 and Section 3.3, respectively.

3.1 Experimental Setup

Experiments were conducted on a workstation featuring an Intel(R) Core(TM) i9-8950HK @ 2.90GHz CPU, 32 GB of RAM, and an NVIDIA GTX1050 Ti GPU with 4GB of memory. All implementations and experimental evaluations were executed using MATLAB R2021b.

This study intentionally omitted image augmentation to focus exclusively on extracting pure features from the original images.

The testing strategy employed a 5-fold cross-validation approach. This method ensures statistical reliability by repeatedly training and testing on the same dataset. Specifically, the dataset is divided into 80% for training and 20% for testing at each iteration.

3.2 Results with HC features

The results of training the classifiers with HC features are shown in Tables 2 to 5. They show the results with DT, kNN, RF, and SVM, respectively.

As shown in Table 2, the DT classifier shows accuracy scores from 58.06% (ZM) to 71.32% (LM). The LBP and LM features exhibit the best performance,

Table 2: Performance obtained with DT trained with HC features.

Desc.	A	P	R	S	F1	MCC	BACC
AC	62.78	69.39	68.97	53.26	69.18	22.20	61.12
Haar	59.70	62.56	83.31	23.43	71.46	8.33	53.37
Hist	68.78	74.49	73.71	61.22	74.10	34.84	67.46
HAR	68.78	74.85	72.99	62.32	73.91	35.10	67.66
LBP	71.22	76.23	76.26	63.47	76.25	39.74	69.87
CH_1	71.11	76.15	76.17	63.35	76.16	39.52	69.76
CH_2	71.05	76.12	76.07	63.35	76.09	39.41	69.71
LM	71.32	76.16	76.64	63.16	76.40	39.87	69.90
ZM	58.06	65.74	64.24	48.57	64.98	12.73	56.40

Table 3: Performance obtained with kNN trained with HC features.

Desc.	A	P	R	S	F1	MCC	BACC
AC	57.34	70.04	51.66	66.06	59.46	17.42	58.86
Haar	42.17	56.99	18.40	78.67	27.82	-3.61	48.53
Hist	64.64	71.97	68.15	59.24	70.01	27.07	63.70
HAR	61.06	68.53	66.05	53.41	67.26	19.29	59.73
LBP	69.51	75.32	73.86	62.82	74.58	36.50	68.34
CH_1	66.16	72.41	71.28	58.29	71.84	29.45	64.78
CH_2	65.46	72.09	70.14	58.29	71.10	28.24	64.21
LM	66.32	72.57	71.38	58.55	71.97	29.81	64.97
ZM	57.40	65.03	64.19	46.97	64.60	11.12	55.58

reflecting high precision and BACC, indicating their suitability for DT. Conversely, ZM and Haar features fall short, with lower MCC and specificity values.

kNN (see Table 3) presents accuracy scores vary from 42.17% (Haar) to 69.51% (LBP). Haar features again exhibit subpar performance, particularly in recall and MCC, suggesting they are unsuitable for kNN. LBP features once more demonstrate superior performance, with high precision and BACC.

Regarding the RF classifier (see Table 5), the accuracy scores range from 62.48% (Haar) to 79.57% (LBP), indicating a significant variation in the effectiveness of different features. LBP stands out with the highest accuracy and strong precision, recall, and F1 performance. Conversely, Haar features yield poor specificity and MCC, highlighting their inadequacy for this classifier. Interestingly, the CH_1, CH_2, and LM features consistently perform well, underscoring their reliability with RF.

Finally, SVM (see Table 4) reveals accuracy scores ranging from 44.67% (Hist) to 75.92% (CH_1). CH_1 and LM features lead with notable precision, recall, and F1-score performance, indicating their robustness for SVM. In contrast, Haar and Hist features are less effective, particularly in recall and specificity, which are crucial for SVM’s discriminative power.

3.3 Results with deep features

The results obtained by training the classifiers with deep features are shown in Tables 6 to 9, with DT, kNN, RF, and SVM, respectively.

DT Classifier with deep features (Table 6) obtained accuracy scores ranging from 73.52% (Inception-ResNet-v2) to 84.92% (DenseNet-201). The latter demonstrates excellent precision, recall, and F1-score, indicating its efficacy. Other deep features, like DarkNet-53 and ResNet-50, also perform well.

kNN with deep features, as shown in Table 7, obtained improved results w.r.t. DT since accuracy scores range from 76.13% (Inception-ResNet-v2) to 88.25% (DarkNet-53). DarkNet-53 and DenseNet-201 maintain high precision and recall, indicating their robustness.

Table 4: Performance obtained with SVM trained with HC features.

Desc.	A	P	R	S	F1	MCC	BACC
AC	67.30	69.18	82.99	43.20	75.45	28.71	63.09
Haar	62.18	62.38	94.59	12.38	75.18	12.45	53.49
Hist	44.67	96.29	9.00	99.47	16.47	17.91	54.23
HAR	62.07	73.64	58.21	68.00	65.02	25.64	63.10
LBP	62.64	70.00	67.06	55.85	68.50	22.69	61.46
CH_1	75.92	77.37	85.14	61.75	81.07	48.61	73.45
CH_2	72.50	71.57	90.55	44.76	79.95	40.78	67.66
LM	73.32	72.65	89.73	48.11	80.29	42.61	68.92
ZM	63.84	69.78	71.08	52.72	70.43	23.93	61.90

Table 5: Performance obtained with RF trained with HC features.

Desc.	A	P	R	S	F1	MCC	BACC
AC	71.76	72.89	84.97	51.47	78.47	39.09	68.22
Haar	62.48	62.65	94.22	13.71	75.26	13.61	53.97
Hist	73.26	77.24	79.19	64.15	78.20	43.66	71.67
HAR	76.78	78.69	84.55	64.84	81.52	50.63	74.69
LBP	79.57	80.74	87.03	68.11	83.77	56.61	77.57
CH_1	78.11	79.99	85.17	67.28	82.50	53.56	76.22
CH_2	78.07	79.84	85.34	66.90	82.50	53.43	76.12
LM	78.25	80.20	85.09	67.73	82.58	53.87	76.41
ZM	65.19	68.16	79.84	42.70	73.54	24.26	61.27

The integration of deep features within RF classifier, as detailed in Table 8, results in high accuracy scores, ranging from 83.25% (Inception-ResNet-v2) to 91.93% (DenseNet-201). DenseNet-201 and EfficientNet B0 features stand out with superior performance across all measures, including MCC and BACC, showcasing their robustness. These results suggest that deep features significantly enhance the RF classifier’s performance.

Finally, the SVM results, shown in Table 9, reveal accuracy scores from 69.87% (Inception-ResNet-v2) to 86.02% (DenseNet-201). DenseNet-201 and EfficientNet B0 again lead with high precision, recall, and F1.

3.4 Discussion

Across all classifiers, DenseNet-201 and EfficientNet B0 features consistently deliver superior performance. The RF and kNN classifiers benefit from deep features, achieving high accuracy and balanced performance. Conversely, traditional HC features, while sometimes effective, generally lag behind deep features, emphasizing the shift towards DL-based feature extraction in modern ML workflows. This comprehensive evaluation underscores the importance of selecting appropriate feature sets tailored to specific classifiers to optimize performance

Table 6: Performance obtained with DT trained with deep features.

Desc.	A	P	R	S	F1	MCC	BACC
AlexNet	75.00	79.47	79.19	68.57	79.33	47.72	73.88
DarkNet-19	78.25	82.04	82.04	72.42	82.04	54.46	77.23
DarkNet-53	81.64	84.78	84.95	76.57	84.86	61.55	80.76
DenseNet-201	84.92	87.51	87.60	80.80	87.56	68.42	84.20
EfficientNet B0	78.79	82.62	82.29	73.41	82.46	55.64	77.85
Inception-v3	74.54	79.21	78.60	68.30	78.90	46.81	73.45
Inception-ResNet-v2	73.52	78.02	78.35	66.10	78.18	44.49	72.22
ResNet-18	76.73	81.20	80.13	71.50	80.66	51.46	75.82
ResNet-50	81.30	84.62	84.47	76.42	84.55	60.87	80.45
ResNet-101	80.13	83.67	83.48	74.97	83.58	58.42	79.23
VGG19	76.40	80.97	79.79	71.20	80.37	50.80	75.49
Xception	79.38	83.30	82.49	74.59	82.89	56.94	78.54

outcomes. Also, it demonstrates that the task at hand can be faced with general-purpose features without specific fine-tuning strategies.

Compared to the reference results provided by the dataset’s authors, we achieved results comparable to those obtained with end-to-end fine-tuned DL methods in this work. For example, the RF classifier reached a maximum F1 of 93.4%, being only 3% lower than the best result obtained in [7] with a fine-tuned ResNet-50.

4 Conclusion

In this work, the task of histopathological image classification has been faced with a comprehensive analysis of several different HC and deep features used

Table 7: Performance obtained with kNN trained with deep features.

Desc.	A	P	R	S	F1	MCC	BACC
AlexNet	80.85	83.80	84.77	74.82	84.28	59.78	79.80
DarkNet-19	83.99	86.47	87.20	79.05	86.84	66.40	83.13
DarkNet-53	88.25	88.89	92.11	82.32	90.48	75.25	87.22
DenseNet-201	88.21	89.04	91.84	82.63	90.42	75.16	87.23
EfficientNet B0	87.53	89.01	90.60	82.82	89.80	73.79	86.71
Inception-ResNet-v2	76.13	79.89	80.98	68.69	80.43	49.85	74.83
Inception-v3	80.88	83.65	85.04	74.48	84.34	59.80	79.76
ResNet-101	87.89	88.57	91.87	81.79	90.19	74.48	86.83
ResNet-18	84.21	85.89	88.47	77.68	87.16	66.73	83.07
ResNet-50	86.97	88.20	91.09	80.41	89.62	73.19	85.75
VGG19	83.35	85.94	86.94	77.95	86.44	65.88	82.45
Xception	85.15	86.74	89.44	78.95	88.07	70.17	84.20

Table 8: Performance obtained with RF trained with deep features.

Desc.	A	P	R	S	F1	MCC	BACC
AlexNet	84.02	85.55	88.57	77.03	87.03	66.29	82.80
DarkNet-19	88.30	88.68	92.49	81.87	90.54	75.33	87.18
DarkNet-53	90.30	90.72	93.55	85.30	92.11	79.58	89.42
DenseNet-201	91.93	92.61	94.20	88.46	93.40	83.05	91.33
EfficientNet B0	89.89	89.96	93.77	83.92	91.83	78.71	88.85
Inception-v3	85.52	85.64	91.42	76.46	88.44	69.39	83.94
Inception-ResNet-v2	83.25	84.10	89.21	74.10	86.58	64.55	81.65
ResNet-18	86.99	87.32	91.87	79.50	89.53	72.54	85.68
ResNet-50	89.92	90.12	93.63	84.23	91.84	78.77	88.93
ResNet-101	89.59	89.76	93.48	83.62	91.58	78.07	88.55
VGG19	85.98	86.61	90.92	78.40	88.71	70.41	84.66
Xception	88.58	89.08	92.49	82.59	90.75	75.94	87.54

Table 9: Performance obtained with SVM trained with deep features.

Desc.	A	P	R	S	F1	MCC	BACC
AlexNet	72.97	77.49	76.56	65.81	77.02	42.80	71.18
DarkNet-19	77.86	82.20	80.82	71.95	81.50	53.28	76.39
DarkNet-53	82.83	85.84	84.99	76.88	85.41	63.65	80.94
DenseNet-201	86.02	89.01	86.61	81.84	87.79	69.91	84.23
EfficientNet B0	82.84	85.76	85.35	76.96	85.55	63.48	81.15
Inception-v3	73.60	78.88	74.73	67.51	76.75	45.86	71.12
Inception-ResNet-v2	69.87	75.03	71.65	62.78	73.29	35.68	67.21
ResNet-18	77.78	82.17	80.82	71.86	81.49	53.13	76.34
ResNet-50	82.77	86.11	84.34	77.87	85.22	63.43	81.11
ResNet-101	82.52	85.76	84.71	76.81	85.23	63.00	80.76
VGG19	79.60	83.94	81.78	73.70	82.84	57.67	77.74
XceptionNet	82.24	85.75	84.22	76.22	84.97	62.53	80.22

to train four different ML classifiers. We have shown that deep features, like those extracted from DenseNet-201 and EfficientNet B0, obtained superior performance than HC, demonstrating the power of advanced CNN architectures in extracting relevant features for classification tasks. An RF classifier reached a maximum F1 of 93.4%, highlighting the efficacy of our approach in achieving competitive results without fine-tuning more complex systems.

Despite these promising results, future work will extend classification to include feature merging and further classifiers, incorporating Vision Transformers. Additionally, further developments will address cross-dataset issues through testing and potential refinements on new datasets and different types of staining.

References

- [1] Abul Abbas Barbhuiya, Ram Kumar Karsh, and Rahul Jain. “CNN based feature extraction and classification for sign language”. en. In: *Multimedia Tools and Applications* 80.2 (Jan. 2021), pp. 3051–3069. ISSN: 1573-7721. DOI: 10.1007/s11042-020-09829-y. URL: <https://doi.org/10.1007/s11042-020-09829-y> (visited on 11/07/2023).
- [2] Jyostna Bodapati and N. Veeranjanyulu. “Feature Extraction and Classification Using Deep Convolutional Neural Networks”. In: *Journal of Cyber Security and Mobility* 8 (Jan. 2019), pp. 261–276. DOI: 10.13052/jcsm2245-1439.825.
- [3] Jia Deng et al. *ImageNet: a Large-Scale Hierarchical Image Database*. Journal Abbreviation: IEEE Conference on Computer Vision and Pattern Recognition Pages: 255 Publication Title: IEEE Conference on Computer Vision and Pattern Recognition. IEEE, June 2009. DOI: 10.1109/CVPR.2009.5206848.
- [4] Cecilia Di Ruberto, Lorenzo Putzu, and Giuseppe Rodriguez. “Fast and accurate computation of orthogonal moments for texture analysis”. In: *Pattern Recognition* 83 (Nov. 2018), pp. 498–510. ISSN: 0031-3203. DOI: 10.1016/j.patcog.2018.06.012. URL: <https://www.sciencedirect.com/science/article/pii/S003132031830222X> (visited on 11/06/2023).
- [5] Robert M. Haralick, K. Shanmugam, and Its’Hak Dinstein. “Textural Features for Image Classification”. In: *IEEE Transactions on Systems, Man, and Cybernetics* SMC-3.6 (Nov. 1973). Conference Name: IEEE Transactions on Systems, Man, and Cybernetics, pp. 610–621. ISSN: 2168-2909. DOI: 10.1109/TSMC.1973.4309314. URL: <https://ieeexplore.ieee.org/document/4309314> (visited on 11/06/2023).
- [6] Dong-chen He and Li Wang. “Texture Unit, Texture Spectrum, And Texture Analysis”. In: *IEEE Transactions on Geoscience and Remote Sensing* 28.4 (July 1990). Conference Name: IEEE Transactions on Geoscience and Remote Sensing, pp. 509–512. ISSN: 1558-0644. DOI: 10.1109/TGRS.1990.572934. URL: <https://ieeexplore.ieee.org/document/572934> (visited on 11/06/2023).
- [7] Weiming Hu et al. “GasHisSDB: A new gastric histopathology image dataset for computer aided diagnosis of gastric cancer”. In: *Comput. Biol. Medicine* 142 (2022), p. 105207. DOI: 10.1016/J.COMPBIOMED.2021.105207. URL: <https://doi.org/10.1016/j.compbiomed.2021.105207>.
- [8] Milena Ilic and Irena Ilic. “Epidemiology of stomach cancer”. In: *World journal of gastroenterology* 28.12 (2022), p. 1187.
- [9] Rekhil M. Kumar et al. *A Comparative Study of Gastric Histopathology Sub-size Image Classification: from Linear Regression to Visual Transformer*. 2022. arXiv: 2205.12843 [cs.CV]. URL: <https://arxiv.org/abs/2205.12843>.
- [10] J. Mitro. “Content-based image retrieval tutorial”. In: *ArXiv e-prints* (2016).
- [11] R. Mukundan, S.H. Ong, and P.A. Lee. “Image analysis by Tchebichef moments”. In: *IEEE Transactions on Image Processing* 10.9 (Sept. 2001).

- Conference Name: IEEE Transactions on Image Processing, pp. 1357–1364. ISSN: 1941-0042. DOI: 10.1109/83.941859. URL: <https://ieeexplore.ieee.org/document/941859> (visited on 11/06/2023).
- [12] Timo Ojala, Matti Pietikäinen, and Topi Mäenpää. “Multiresolution Gray-Scale and Rotation Invariant Texture Classification with Local Binary Patterns”. In: *IEEE Trans. Pattern Anal. Mach. Intell.* 24.7 (2002), pp. 971–987.
- [13] Mustapha Oujaoura, Brahim Minaoui, and Mohammed Fakir. “Image annotation by moments”. In: *Moments and Moment Invariants-Theory and Applications* 1.10 (2014), pp. 227–252.
- [14] Biserka Petrovska et al. “Deep Learning for Feature Extraction in Remote Sensing: A Case-Study of Aerial Scene Classification”. In: *Sensors* 20.14 (2020), p. 3906.
- [15] Lorenzo Putzu and Cecilia Di Ruberto. “Rotation Invariant Co-occurrence Matrix Features”. en. In: *Image Analysis and Processing - ICIAP 2017*. Ed. by Sebastiano Battiato et al. Lecture Notes in Computer Science. Cham: Springer International Publishing, 2017, pp. 391–401. ISBN: 978-3-319-68560-1. DOI: 10.1007/978-3-319-68560-1_35.
- [16] Lorenzo Putzu, Andrea Loddo, and Cecilia Di Ruberto. “Invariant Moments, Textural and Deep Features for Diagnostic MR and CT Image Retrieval”. In: *Computer Analysis of Images and Patterns: 19th International Conference, CAIP 2021, Virtual Event, September 28–30, 2021, Proceedings, Part I*. Berlin, Heidelberg: Springer-Verlag, Sept. 2021, pp. 287–297.
- [17] Michael Reed Teague. “Image analysis via the general theory of moments*”. In: *J. Opt. Soc. Am.* 70.8 (1980), pp. 920–930.
- [18] C.-H. Teh and R.T. Chin. “On image analysis by the methods of moments”. In: *IEEE Transactions on Pattern Analysis and Machine Intelligence* 10.4 (July 1988). Conference Name: IEEE Transactions on Pattern Analysis and Machine Intelligence, pp. 496–513. ISSN: 1939-3539. DOI: 10.1109/34.3913. URL: <https://ieeexplore.ieee.org/document/3913> (visited on 11/06/2023).
- [19] P. Viola and M. Jones. “Rapid object detection using a boosted cascade of simple features”. In: *Proceedings of the 2001 IEEE Computer Society Conference on Computer Vision and Pattern Recognition. CVPR 2001*. Vol. 1. Dec. 2001, pp. I–I.